Higgs boson hadronic branching ratios at the ILC

Yambazi Banda, Tomáš Laštovička, and Andrei Nomerotski

University of Oxford,
Denys Wilkinson Building, Keble Road,
Oxford OX1 3RH, UK

We present a study of the Higgs boson decay branching ratios to $b\bar{b}$, $c\bar{c}$ and gluons, one of the cornerstones of the physics program at the International Linear Collider (ILC). A standard model Higgs boson of 120 GeV mass, produced in the Higgs-strahlung process at $\sqrt{s} = 250$ GeV was investigated using the full detector simulation and reconstruction procedures. The analysis was performed in the framework of the Silicon Detector (SiD) concept with full account of inclusive standard model backgrounds. The selected decay modes contained two heavy flavour jets in the final state and required excellent flavour tagging through precise reconstruction of interaction and decay vertices in the detector. A new signal discrimination technique using correlations of neural network outputs was used to determine the branching ratios and estimate their uncertainties, 4.8%, 8.4% and 12.2% for $b\bar{b}$, $c\bar{c}$ and gluons respectively.

I. INTRODUCTION

The measurement of the Higgs absolute branching ratios in all possible decay modes is one of the most important parts of the ILC program, giving a precision test of the standard model (SM) prediction that the Higgs boson couples to each particle in proportion to its mass [1]. While the Large Hadron Collider (LHC) is a likely discovery machine for the Higgs boson it will be almost impossible to determine the total Higgs cross section there, making it difficult to make absolute measurements of partial decay widths. On the other hand, precise and model independent measurements of absolute branching ratios can be performed at the ILC [2].

In this paper the Higgs decay modes to charm quarks, bottom quarks and gluons which result in two and four-jet final states are considered. Heavy quarks, b and c, couple directly to the Higgs while the Higgs decay to gluons in the standard model is mediated by heavy quark loops. The branching ratio to gluons is indirectly related to $t\bar{t}H$ Yukawa coupling [3] and would probe the existence of new strongly interacting particles that couple to the Higgs and are too heavy to be produced directly. The precise measurements of the branching ratios will help to discriminate between different 'Beyond the SM' (BSM) scenarios [4, 5] where the Higgs couplings differ from SM Higgs couplings.

The production cross sections, branching ratios and decay widths of the Higgs are determined by the strength of the Yukawa couplings to fermions and gauge bosons, whose scale is set by the masses of these particles. For a Higgs boson mass of 120 GeV, the expected branching ratios to bottom quarks, charm quarks and gluons are 67.9%, 3.1% and 7.1%, respectively.

While the Higgs branching ratios in the e^+e^- collider environment has been studied before [6], up to date it was done in a parametric way from the detector point of view, without exploiting full Monte Carlo (MC) simulations nor realistic reconstruction algorithms. It should

be noted that this measurement is a complex analysis which heavily relies on the bottom and charm quark tagging. Possible detector resolution and acceptance effects together with non-ideal efficiency and purity of the reconstruction algorithms could play a critical role in the ultimate sensitivity of the experiment and hence in its physics reach. This study for the first time addresses these issues in the framework of the Silicon Detector (SiD) concept as one of the benchmarking analyses prepared for the SiD Letter of Intent [7]. A new technique employing two neural networks was used to overcome one of the main difficulties of the analysis: separation of signal from the background of Higgs decays to other particles.

The paper is organized as follows: the Higgs boson production at the ILC and the SiD detector concept are introduced in Section II; Sections III and IV describe the details of the analysis and its results, which are summarized in Section V.

II. HIGGS PRODUCTION AT THE ILC

A. The ILC

The ILC is a next generation electron-positron accelerator designed to collide particles at the centre-of-mass energy up to 500 GeV, upgradeable to 1 TeV, with peak luminosity of 2×10^{34} cm^{-2}s^{-1}. The dominant production mechanisms for the SM Higgs at e^+e^- colliders are Higgs-strahlung [8, 9], WW and ZZ fusion processes [10]

$$
\begin{aligned}
e^+e^- &\to ZH \to f\bar{f}H \\
e^+e^- &\to \nu\bar{\nu}W^*W^* \to \nu\bar{\nu}H \\
e^+e^- &\to e^+e^-Z^*Z^* \to e^+e^-H.
\end{aligned}
\tag{1}
$$

The Higgs-strahlung and WW fusion processes are both capable of generating $\nu\bar{\nu}H$ states.

B. The SiD Detector Concept

The sensitivity to Higgs decay branching ratios measurement was studied in the framework of the Silicon Detector (SiD) concept [7] using full detector simulation and event reconstruction. SiD is designed for precision measurements of a wide range of possible new phenomena at the ILC. It is based on a silicon pixel vertex detector, silicon tracking, silicon-tungsten electromagnetic calorimetry, and highly segmented hadronic calorimetry. The Particle Flow Algorithm (PFA) approach [7] is an important strategy driving the basic philosophy and layout of the detector. SiD also incorporates a 5 T solenoid, iron flux return and a muon identification system. A schematic view of SiD quadrant is shown in Figure 1.

The vertex detector comprises a central barrel with five silicon pixel layers and four silicon pixel disks for the forward and backward regions providing the impact parameter resolution of $5 \oplus 10/(p \sin^{3/2} \theta)$ [μm] and good hermeticity for $\cos \theta \leq 0.984$ where θ is the polar angle.

SiD has adopted silicon strip technology for its tracker, arranged in five cylinders and four endcaps necessary for precision tracking and momentum measurement. Given an outer cylinder radius of 1.25 m, the charged track momentum resolution is expected to be better than $\sigma(1/p_T) = 5 \times 10^{-5}$ (GeV/c)$^{-1}$ for high momentum tracks.

Calorimetry in SiD is optimized for jet energy measurements, and is based on the Particle Flow strategy, in which the momenta of charged particles are measured in the tracker; the momenta of neutrals are measured in the calorimeters, and then the charged and neutral components are combined. The SiD calorimetry begins with a dense, highly pixelated silicon-tungsten electromagnetic calorimeter with energy resolution of $17\%/\sqrt{E}$. The Hadronic Calorimeter (HCAL) is composed of 4.5λ HCAL depth of stainless steel, divided into 40 layers of steel and detector. A good jet energy resolution, about 4%, allows the invariant masses of W's, Z's and top quarks to be reconstructed with resolution nearing the natural widths of these particles.

III. ANALYSIS

A. Analysis Framework

Both the signal and background events were produced at the centre-of-mass energy $\sqrt{s} = 250$ GeV, total integrated luminosity of 250 fb^{-1} and the Higgs mass of 120 GeV. The choice of energy in this analysis maximizes the cross-section value for Higgs-strahlung. Only HZ process was considered as it accounts for about 95% of the total $Hf\bar{f}$ cross section for this energy and Higgs mass choices. SM events (mainly WW, ZZ and qq pairs) and Higgs decays to fermions other than the signal were considered as backgrounds. All 0, 2 and 4 fermion final states were generated using the WHIZARD Monte Carlo Event Generator [11] taking into account beamstrahlung and initial state radiation (ISR) photons [7]. PYTHIA [12] was used for the final state QED and QCD parton showering, fragmentation and decay to provide final-state observable particles. For this study, event samples were created conforming to the expected ILC baseline parameters of $\pm 80\%$ electron and $\mp 30\%$ positron polarization. About 7M events were processed through the full detector simulation, with individual events weighted to reflect the statistical sampling.

The detector response to generated events was simulated using the Geant4 toolkit [13, 14], which provided the necessary classes to describe the geometry of the detector, the transport and interaction of particles with materials and fields. A thin layer of Linear Collider specific code, SLIC [15], provided access to the Monte Carlo events, the detector geometry and the output of the detector hits. The detector parameters could be varied without having to rebuild the simulation executable binaries since the geometries were fully described at runtime. The output was in the standard LCIO format [16] so that detector concepts using other simulation packages could be studied and data generated using this system can be analyzed in other analysis frameworks.

The identification of jets is an important part of this analysis. The fragmentation products of the hadronic systems were forced either to two or four jets, depending on the final state, using the DURHAM algorithm [17]. To provide the most probable kinematic configuration of the event topology, a kinematic fitter, Marlin Kinfit [18], with four-momenta and mass constraints was used. The fitter uses the method of Lagrange multipliers to determine the most probable value for the jet four-momentum.

In order to identify primary, secondary and tertiary vertices the topological vertex finder ZVTOP was utilized. The algorithm is part of a vertexing package developed by the LCFI collaboration [19]. It classifies events on the number of found vertices and combines eight optimized variables for each type of event in a neural network, which is then separately trained on samples of b, c and light quarks. The best discriminating variables were the corrected vertex mass, secondary vertex probability, impact parameter significance and the number of vertices in the event.

B. Event Selection

The analysis signature is dependent on the Z boson decay products (charged leptons, hadrons or neutrinos). The channels studied in this analysis were the neutrino mode (Z decaying to neutrinos) and the hadronic mode (Z decaying to hadrons), referred below as the signal.

The events were classified into the two channels using the number of leptons and visible energy in the event. The leptons were defined as reconstructed electrons or muons with momenta larger than 15 GeV. The visible energy was defined as the sum of energies of all recon-

FIG. 1. A plane view of a quadrant of SiD. Dimensions are in mm.

structed particles [7] in the event. Figure 2 shows the distributions of the visible energy and the number of leptons for the signal, Higgs background and SM background before any selections, normalized to $250\,\mathrm{fb}^{-1}$.

In the neutrino mode, events not having leptons and with visible energy in the 90 to $160\,\mathrm{GeV}$ interval were selected. In this channel all reconstructed particles were clustered into two jets which, for the signal, were assumed to come from the Higgs boson recoiling against two neutrinos from the Z boson decay. The most important backgrounds in this channel were two-fermion events, ZZ pairs decaying to neutrinos and hadrons, and WW pairs where one W decays hadronically and the other W decays into a neutrino and a lepton, which escapes undetected.

A cut based selection was performed to further reduce the backgrounds in this channel using kinematic variables described below. The transverse momentum of each jet, p_T, was calculated to reject SM background events which are softer compared to signal events. The number

of tracks per jet, n_{tracks}, was used to reject purely leptonic events which were not part of the signal. The discrimination between the signal and backgrounds with a different number of jets was achieved by the y_{min} parameter, which corresponds to the minimum y-parameter for the two jet hypothesis in the DURHAM algorithm. The variable $-\log(y_{min})$ was used to exclude fully hadronic WW (and ZZ) events, which were four-jet events misidentified as two-jet events. Thrust [20] values were calculated since it is expected that signal events are less boosted and are more spherical than the background events. Values of $|\cos(\theta_{thrust})|$ were also used because signal events are expected to be produced more centrally in the detector while majority of the background processes have a strongly forward peaking angular distribution. A large fraction of background events have back-to-back jets whereas signal events were confined to a range of angular values due to kinematic constraints coming from ZH production. The di-jet invariant mass was used to reject low mass hadronic systems from WW, ZZ and
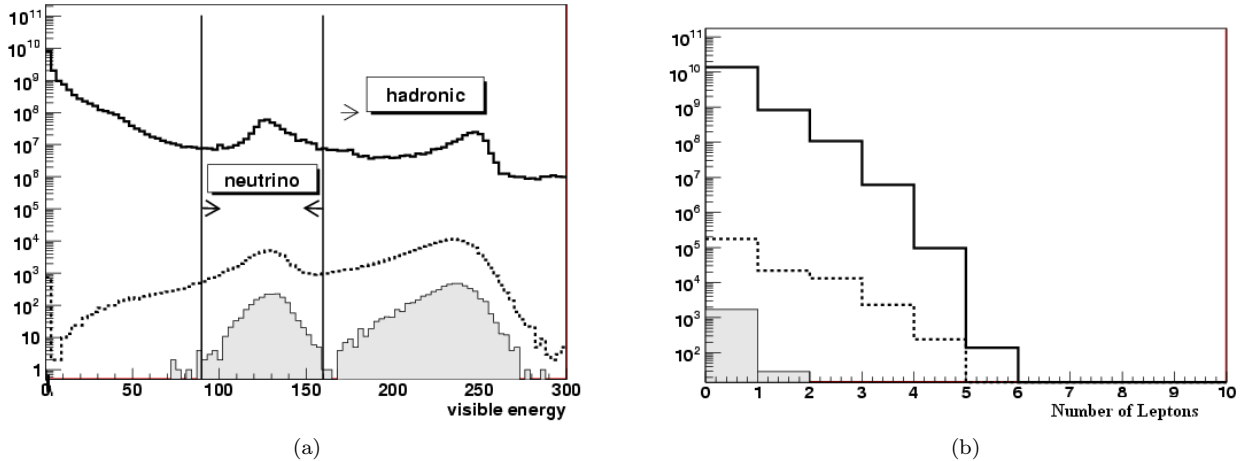
FIG. 2. Visible energy (a) and the number of leptons per event (b) used for channel classification. Solid curves are SM background, dashed curves are inclusive Higgs sample and filled histograms are the signals. All histograms are normalized to $250 \, \text{fb}^{-1}$.

two-photon events. The signal events rarely have hard photons and this helps reject both highly energetic initial state radiation (ISR) photons and hard photons from di-jet events which occur for the background. No photon isolation was required in this particular case. Figure 3 shows some of the distributions for the above variables used in the neutrino channel before any selections.

The hadronic mode was selected as events with no leptons and the visible energy above 170 GeV. In this channel, events were forced to have four reconstructed jets. For the signal, two of the jets were required to have their di-jet invariant mass consistent with the Higgs boson and the other two having the mass consistent with the Z boson mass. The main backgrounds for this channel were WW and ZZ pairs where the all bosons decay to hadrons. For the pre-selection, we used kinematic selections defined similar to the ones in the neutrino channel. The full list of selections in the neutrino and hadronic channels is given in Tables I and II. Table III instead shows the number of events before and after pre-selection cuts for $c\bar{c}$, $b\bar{b}$ and gg modes in the neutrino and hadronic channels before and after pre-selection cuts. The number of events for the SM background is indicated in the same table.

As mentioned before, the LCFI vertexing package was used for vertex finding and identification of the flavour of hadrons in jets. The flavour identification is essential to differentiate b jets from c jets and jets coming from light (u, d, s) quark hadronization. In analyses like the present

one where multi-b states are to be separated from significant backgrounds, a high b-tagging efficiency is required to discriminate against light and c-quarks. Furthermore, the measurement of the $H \to c\bar{c}$ branching ratio requires efficient c-tagging with high rejection of b-quarks. The package produces three possible flavour tags, 'b-tag', 'c-tag' and 'c-tag on b-background only', for each jet in the event. Figure 4 shows the distribution of these variables for the leading jet in the hadron channel for the $c\bar{c}$ decay mode after preselections.

The remaining events were categorized using the neural networks implemented in FANN [21]. The neural network (NN) used optimized sets of 18 input variables for the neutrino channel and of 19 input variables for the hadronic channel. The neural net was constructed out of three hidden layers with 28 neurons and had one output neuron. For $c\bar{c}$ and $b\bar{b}$ signals, the first NN was trained to distinguish the SM background from the inclusive Higgs sample and to produce the $\text{NN}_{SM-Higgs}$ output. In the gg case, the first NN was trained to distinguish the signal sample from the SM background and to produce the NN_{Sig-SM} output. The second NN was, in all cases, trained to distinguish the signal from the Higgs inclusive background sample and to produce the $\text{NN}_{Higgs-signal}$ output. The training was done separately for $c\bar{c}$, $b\bar{b}$ and for gg using independent samples. Figure 5 shows an example of distributions of the first and second NNs in the $c\bar{c}$ decay mode for the neutrino channel. For the $c\bar{c}/b\bar{b}/gg$ scenarios the signal was defined as $H \to c\bar{c}/b\bar{b}/gg$ events only and the Higgs background included all Higgs decays other than the signal ones.

The final event samples were determined using a simultaneous selection on the first and second neural nets as specified in Table IV. The selection was performed separately for each channel and decay mode by finding an optimal point at which the signal cross section un-
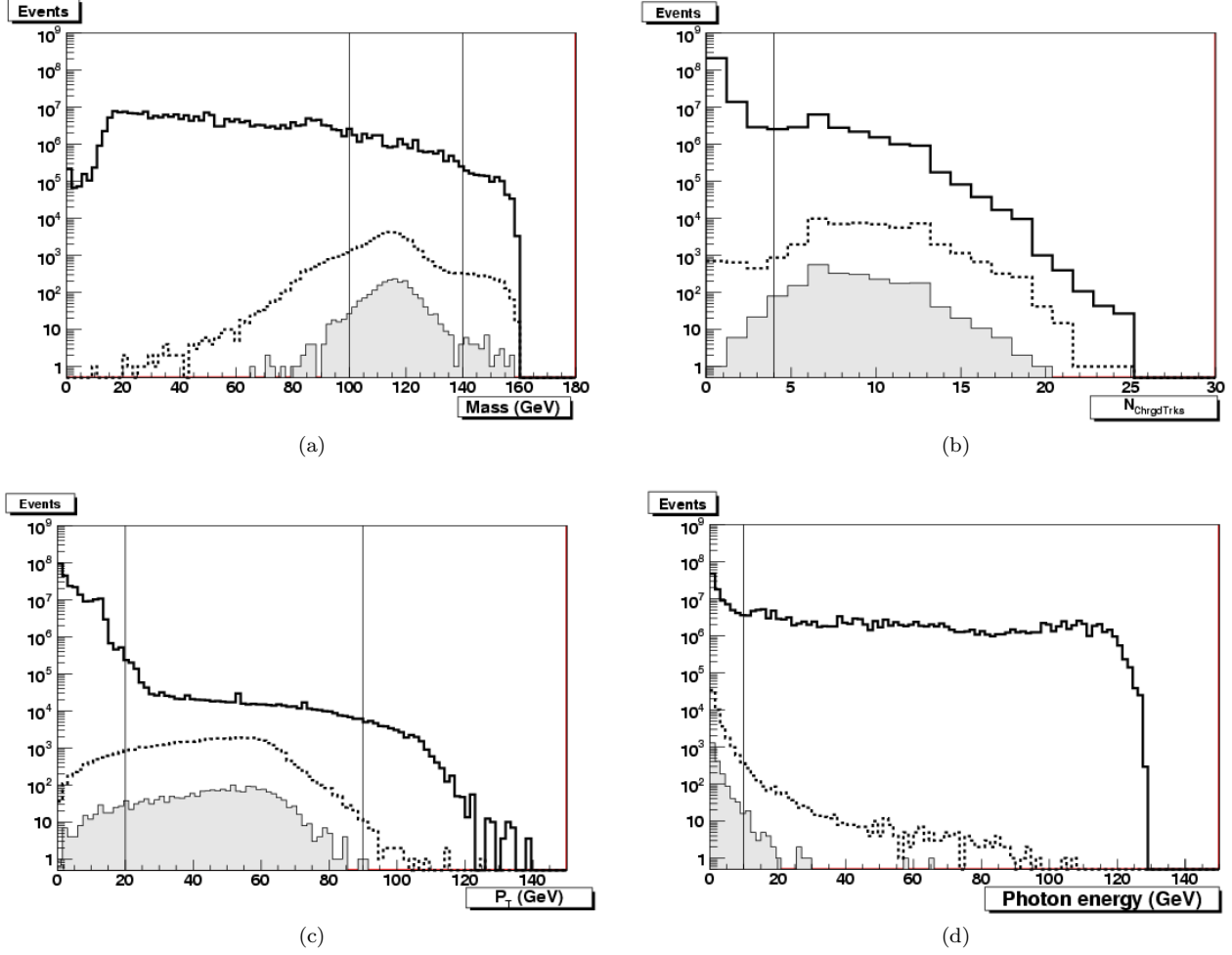
FIG. 3. Distributions of pre-selection kinematic variables in the neutrino channel: (a) di-jet invariant mass, (b) number of charged tracks in the event, (c) jet p_T, (d) highest reconstructed photon energy in the event. Solid curves are the SM background, dashed curves are the Higgs background and filled histograms represent the signal. All histograms are normalized to $250\,\mathrm{fb}^{-1}$ and are shown before any selections.

	selection	value
(1) 20	$<$ p$_T$ of jet	$<$ 90 GeV
(2) 4	$<$ number of charged tracks per jet	
(3)	$-\log(y_{min})$	$<$ 0.8
(4)	thrust	$<$ 0.95
(5)	$\cos(\theta_{thrust})$	$<$ 0.98
(6) 100°	$<$ angle between jets	$<$ 170°
(7) 100 GeV	$<$ di-jet invariant mass	$<$ 140 GeV
(8)	Highest reconstructed photon energy	$<$ 10 GeV

TABLE I. Selections for the neutrino channel.

certainty was minimized. A detailed account of event selections and variable distributions for all decay modes in both channels is given in [22–24].

IV. BRANCHING RATIO CALCULATION

The branching ratio of the Higgs boson decay were calculated using events that passed the final neural network selection. The calculation was done by normalising the signal cross section to the inclusive Higgs cross section,

	selection	value
(1) 4	< number of charged tracks per jet	
(2)	$-\log(y_{min})$	< 2.7
(3)	thrust	< 0.95
(4)	$\cos(\theta_{thrust})$	< 0.96
(5) 105°	< angle between jet 1 and 3	< 165°
(6) 70°	< angle between jet 2 and 4	< 160°
(7) 110 GeV	< invariant mass of Higgs candidate after fit	< 140 GeV
(8) 80 GeV	< invariant mass of Z candidate after fit	< 110 GeV
(9)	Highest reconstructed photon energy	< 10 GeV

TABLE II. Selections for the hadronic channel. The jets are ranked in the decreasing energy order.

		SM	$H \to c\bar{c}$	$H \to b\bar{b}$	$H \to gg$
Neutrino Channel	Before	45936973	637	11580	986
	After	109057	506	6707	759
Hadronic Channel	Before	39398366	1837	30985	2965
	After	967312	947	15805	1611

TABLE III. Number of events before and after pre-selections in the neutrino and hadronic modes.

Decay Mode	Neutrino		Hadronic	
	NN1 >	NN2 >	NN1 >	NN2 >
$c\bar{c}$	0.33	0.38	0.36	0.29
$b\bar{b}$	0.81	0.92	0.64	0.88
gg	0.71	0.87	0.10	0.27

TABLE IV. Neural net selections in the neutrino and hadronic channels.

σ_{ZH} = 209.0±9.8 fb, as determined in an independent recoil mass analysis performed for the SiD Letter of Intent [7]. The branching ratio is then given by

$$BR(H \to f\bar{f}) = \frac{\sigma_{H \to f\bar{f}}}{\sigma_{ZH} \times BR(Z \to q\bar{q}, \nu\bar{\nu})} \quad (2)$$

where $\sigma_{H \to ff}$ is the signal cross section and $BR(Z \to q\bar{q}, \nu\bar{\nu})$ is the decay branching ratio of the Z boson into two jets or neutrinos depending on the channel. $BR(Z \to q\bar{q}, \nu\bar{\nu})$ values were taken from the generator tables. The cross section was calculated as follows:

$$\sigma_{H \to f\bar{f}} = \frac{N}{\varepsilon L} \quad (3)$$

where N was the number of signal events after all selections, ε was the total signal efficiency and L was the integrated luminosity. The cross section uncertainty took into account statistical fluctuations in the number of both signal and background events. Calculation of $BR(H \to gg)$ follows exactly the same procedure.

Summary of the results obtained for both neutrino and hadronic channels is given in Table V. It shows the number of events after all selections, signal efficiency, cross section and the branching ratios with their uncertainties for each channel separately and in combination. The cross sections and branching ratios, determined for combinations of neutrino and hadronic channels, and their relative uncertainties were calculated assuming that the two channels were statistically independent. The uncertainty of the cross section was considered to be of purely statistical nature while the uncertainty of the branching ratio also took into account the total Higgs-strahlung cross section uncertainty, which is correlated for both channels and is the largest source of systematic uncertainty in the analysis. Other systematic uncertainties originating from $BR(Z \to q\bar{q}, \nu\bar{\nu})$ and luminosity uncertainties are of the order of 0.1% and were neglected. The efficiency was derived using larger signal samples and was assumed not to contribute to the uncertainty. Systematic uncertainties originating from the detector properties, reconstruction algorithms and from the polarization measurement uncertainty were not addressed in this study though they are expected to be small.

The branching ratios were measured as 3.3%, 68.2% and 7.4% for $c\bar{c}$, $b\bar{b}$ and gg respectively. It was found that deviations of the determined branching ratios from the values used in the MC generator were within the statistical uncertainties in all cases implying that the analysis did not bias the measurement. The relative uncertainties on the branching ratios were determined to be equal to 8.4%, 4.8% and 12.2% for $c\bar{c}$, $b\bar{b}$ and gg respectively. For the $c\bar{c}$ and gg measurements, the relative uncertainty of the signal cross section dominated the uncertainty of the branching ratio. However, for the main decay channel, $b\bar{b}$, the branching ratio uncertainty was dominated by the uncertainty on the inclusive Higgs-strahlung cross section used for normalization.

The obtained results were found largely consistent with results from earlier studies in [25], [26] and [6], which all used simplified approaches either to the simulation, or reconstruction, or both. The deterioration of sensitivity due to the added realism was recovered with a new signal discrimination technique which utilizes correlations of two neural networks.
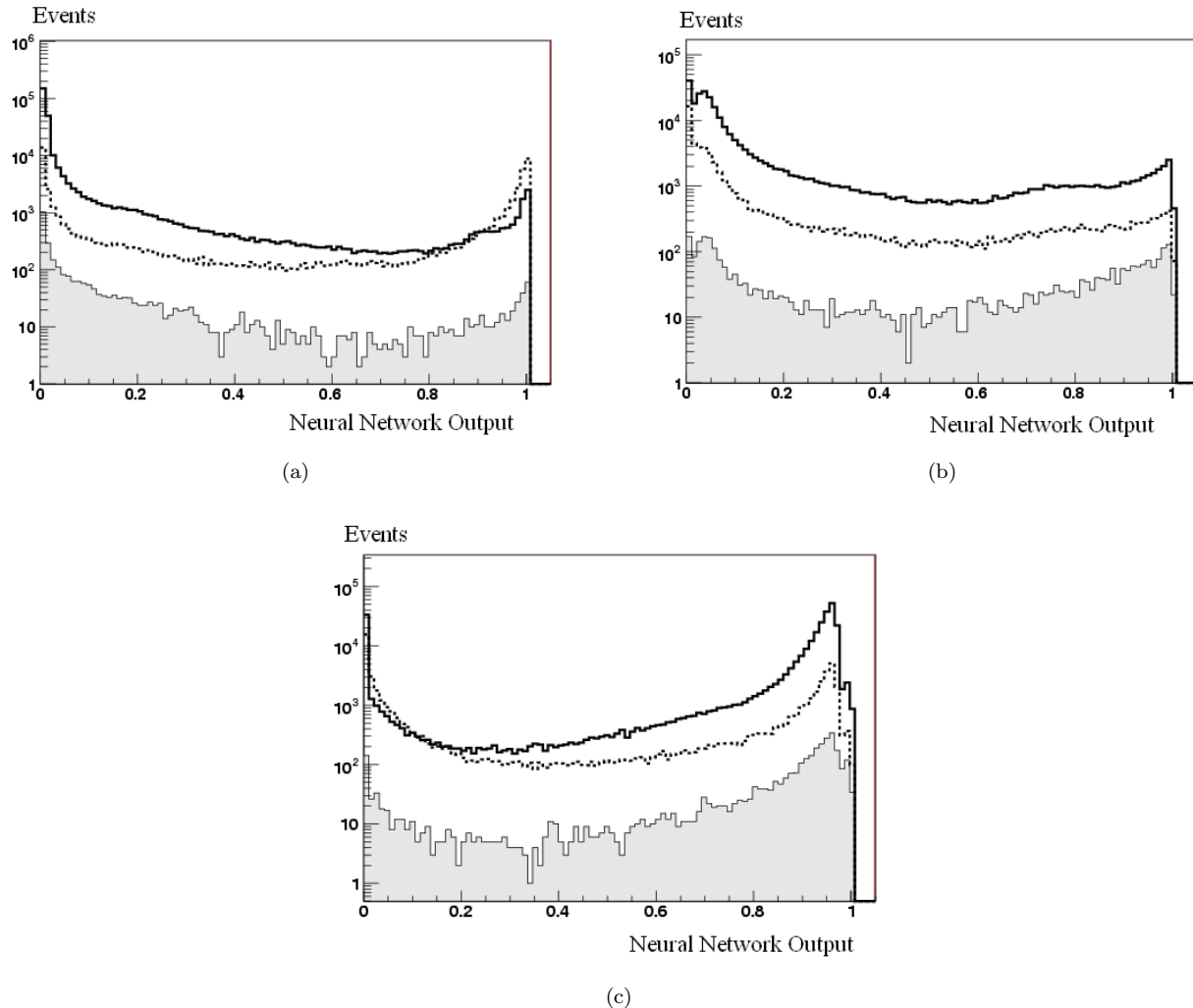
(a)

(b)

(c)

FIG. 4. LCFI flavour tag distributions for the leading jet in the hadronic channel for the $c\bar{c}$ decay mode: (a) b-tagging variable, (b) c-tagging variable and (c) c-tagging variable for the case of b-background only. Solid curves are SM background, dashed curves are Higgs background sample and filled histograms are the signal. All histograms are normalized to $250\,\mathrm{fb}^{-1}$ and are show after preselections.

V.   SUMMARY

The sensitivity to the decay branching ratios of a neutral 120 GeV SM Higgs boson to charm quarks, bottom quarks and gluons has been studied at the ILC centre-of-mass energy of $\sqrt{s} = 250$ GeV and integrated luminosity of 250 fb^{-1}. The analysis is based on full simulation and realistic event reconstruction in the SiD detector and also fully accounts for the standard model background processes. The relative uncertainties obtained are comparable to values obtained in some of the previous studies. Good performance of flavour tagging and the use of neural networks in event selection were critical in obtaining these results. The uncertainties on the branching ratios were found to be equal to 8.4%, 4.8% and 12.2% for $c\bar{c}$, $b\bar{b}$ and gg, respectively. The uncertainty in the $b\bar{b}$ branching ratio is dominated by the uncertainty on the inclusive Higgs-strahlung cross section.
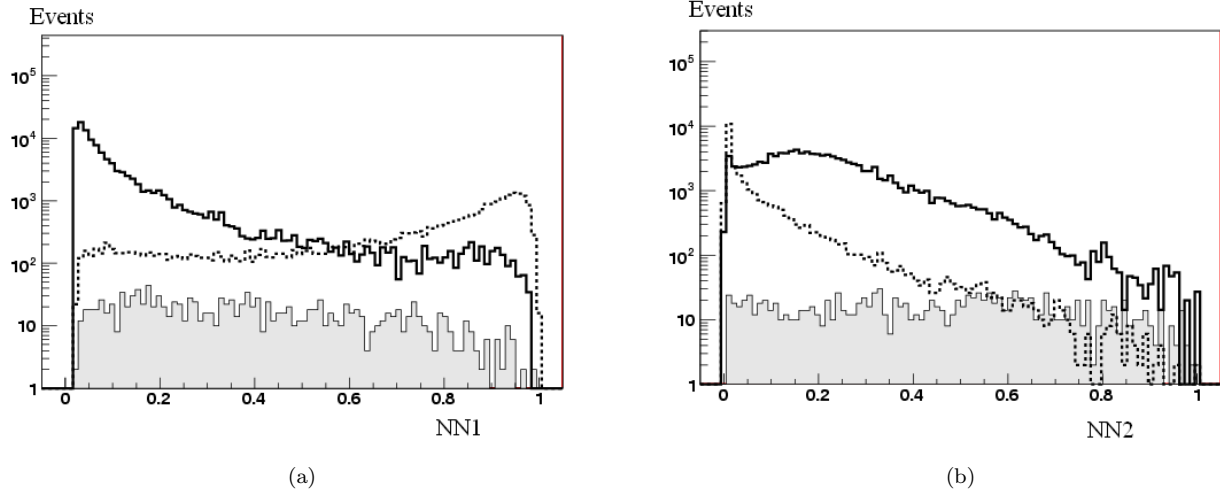
FIG. 5. Neural network outputs in the $c\bar{c}$ decay mode for the neutrino channel: (a) First NN and (b) second NN. Solid curves are SM background, dashed curves are Higgs background sample and filled histograms are the signal. All histograms are normalized to $250\,\mathrm{fb}^{-1}$.

		Neutrino	Hadronic	Combined
$H \rightarrow c\bar{c}$	Signal events	178	407	
	SM background events	140	673	
	Higgs background events	109	213	
	Signal efficiency	27.9	22.2	
	Signal $\sigma_{H \rightarrow c\bar{c}}$	6.8 ± 0.8 fb	6.9 ± 0.6 fb	6.86 ± 0.48 fb
	Relative uncertainty on $\sigma_{H \rightarrow c\bar{c}}$	11.6%	8.8%	7.0%
	Higgs BR	3.3±0.4%	3.3±0.3%	3.3±0.3%
	Relative uncertainty on Higgs BR	12.5%	10.0%	8.4%
$H \rightarrow b\bar{b}$	Signal events	2833	8122	
	SM background events	220	4700	
	Higgs background events	55	423	
	Signal efficiency	24.5	26.2	
	Signal $\sigma_{H \rightarrow b\bar{b}}$	142.7 ± 2.3 fb	142.5 ± 1.9 fb	142.57 ± 1.61 fb
	Relative uncertainty on $\sigma_{H \rightarrow b\bar{b}}$	1.9%	1.4%	1.1%
	Higgs BR	68.3±3.4%	68.2±3.3%	68.2±5.3%
	Relative uncertainty on Higgs BR	5.0%	4.9%	4.8%
$H \rightarrow gg$	Signal events	32	524	
	SM background events	0	3621	
	Higgs background events	4	1431	
	Signal efficiency	3.3	17.7	
	Signal $\sigma_{H \rightarrow gg}$	15.1 ± 1.9 fb	15.6 ± 2.6 fb	15.41 ± 1.74 fb
	Relative uncertainty on $\sigma_{H \rightarrow gg}$	18.7%	14.2%	11.3%
	Higgs BR	7.2±1.4%	7.5±1.1%	7.4±0.9%
	Relative uncertainty on Higgs BR	19.3%	15.0%	12.2%

TABLE V. Results for the $H \rightarrow c\bar{c}$, $H \rightarrow b\bar{b}$ and $H \rightarrow gg$ decay modes.

[1] P. Higgs, Phys. Rev. Lett. **13**, 508 (1964).

[2] G. Weiglein and *et al.* (LHC/ILC Study Group), Phys. Rept. **426**, 47 (2006).

[3] A. Djouadi, M. Spira, and P. Zerwas, Phys. Lett. **B 264** (1991).

[4] M. Battaglia, "Measuring higgs branching ratios and telling the sm from a mssm higgs boson at the e+e- linear collider," ArXiv:hep-ph/9910271.

[5] M. Carena, H. Haber, H. Logan, and S. Mrenna, "Distinguishing a mssm higgs boson from the sm higgs boson at a linear collider," ArXiv:hep-ph/0106116.

[6] T. Kuhl and K. Desch, "Simulation of the measurement of the hadronic branching ratios for a light higgs boson at the ilc," LC-PHSM-2007-001.

[7] *SiD Letter of Intent*, edited by H. Aihara, P. Burrows, and M. Oreglia (2009) arXiv:0911.0006v1.

[8] B. Lee, C. Quigg, and H. Thacker, Phys. Rev. **D 16**, 1519 (1977).

[9] J. Ellis, M. Gaillard, and D. Nanopoulos, Nucl. Phys. **B 106**, 292 (1976).

[10] R. Cahn and S. Dawson, Phys. Lett. **B 136**, 196 (1984).

[11] W. Kilian, T. Ohl, and J. Reuter, "Whizard: Simulating multiple particle processes at lhc and ilc," ArXiv:0708.4233.

[12] T. Sjostrand, S. Mrenna, and P. Skands, JHEP **026** (2006).

[13] S. Agostinelli and *et al*, Nucl. Instrum. Methods Phys. Res. **A 506**, 250 (2003).

[14] J. Allison and *et al*, IEEE Trans. Nucl. Sci. **53**, 270 (2006).

[15] "Slic," Http://www.lcsim.org/software/slic/doxygen/html/.

[16] F. Gaede, T. Behnke, N. Graf, and T. Johnson, "Lcio - a persistency framework for linear collider simulation studies," LC-TOOL-2003-053.

[17] S. Catani, Y. Dokshitzer, M. Olsson, G. Turnock, and B. Webber, Phys. Lett. **B 268**, 432 (1991).

[18] B. List and J. List, "Marlinkinfit: An object-oriented kinematic fitting package," LC-TOOL-2009-001.

[19] A. Bailey and *et al.* (LCFI Collaboration), Nucl. Instrum. Methods Phys. Res. **A 610**, 573 (2009).

[20] S. Brandt, *Jet Analysis in Electron-Positron Annihilation Experiments* (Springer Berlin, 1985).

[21] "Fast Artificial Neural Network Library (fann)," Http://leenissen.dk/fann/html/files/fann-h.html.

[22] Y. Banda, T. Lastovicka, and A. Nomerotski, "Measurement of the higgs boson decay branching ratio to charm quarks at the ilc," ArXiv:0909.1052v3.

[23] Y. Banda, T. Lastovicka, and A. Nomerotski, "Precision measurement of higgs decay branching ratios to bottom quarks and gluons at the ilc," ArXiv:1003.1333v1.

[24] Y. Banda, *Determination of the Higgs Boson Branching Ratios at the International Linear Collider*, Ph.D. thesis, University of Oxford (2010).

[25] C. T. Potter, J. E. Brau, and M. Iwasaki, in *Proc. of the APS/DPF/DPB Summmer Study on the Future of Particle Physics (Snowmass 2001)*, eConf C010630, edited by N. Graf (2001) p. 118.

[26] R. Brinkmann and *et al*, "Tesla technical design report," DESY-2001-011.